6430 *Biochemistry* **2010,** *49,* 6430–6439
DOI: 10.1021/bi100239j

BIOCHEMISTRY
including biophysical chemistry & molecular biology
Article

Functionally Important Amino Acids in the *Arabidopsis* Thylakoid Phosphate Transporter: Homology Modeling and Site-Directed Mutagenesis[†]

Lorena Ruiz-Pavón,[‡,△,◇] Patrik M. Karlsson,[‡,△] Jonas Carlsson,[§,¶] Dieter Samyn,[∥,¶] Bengt Persson,[§] Bengt L. Persson,[∥,⊥,#] and Cornelia Spetea*[,‡]

[‡]*Division of Molecular Genetics, and* [§]*Division of Bioinformatics, Department of Physics, Chemistry, and Biology, Linköping University, 581 83 Linköping, Sweden,* [∥]*School of Natural Sciences, Linnaeus University, 391 82 Kalmar, Sweden,* [⊥]*Laboratory of Molecular Cell Biology, Institute of Botany and Microbiology, Katholieke Universiteit Leuven, Leuven, Belgium, and* [#]*Department of Molecular Microbiology, Flanders Institute of Biotechnology, Kasteelpark Arenberg 31, 3001 Leuven-Heverlee, Flanders, Belgium.* [△]*These authors equally contributed to this work.* [¶]*These authors equally contributed to this work.* [◇]*Present address: School of Natural Sciences, Linnaeus University, 391 82 Kalmar, Sweden.*

Received February 17, 2010; Revised Manuscript Received June 17, 2010

ABSTRACT: The anion transporter 1 (ANTR1) from *Arabidopsis thaliana*, homologous to the mammalian members of the solute carrier 17 (SLC17) family, is located in the chloroplast thylakoid membrane. When expressed heterologously in *Escherichia coli*, ANTR1 mediates a Na^+-dependent active transport of inorganic phosphate (P_i). The aim of this study was to identify amino acid residues involved in P_i binding and translocation by ANTR1 and in the Na^+ dependence of its activity. A three-dimensional structural model of ANTR1 was constructed using the crystal structure of glycerol 3-phosphate/phosphate antiporter from *E. coli* as a template. Based on this model and multiple sequence alignments, five highly conserved residues in plant ANTRs and mammalian SLC17 homologues have been selected for site-directed mutagenesis, namely, Arg-120, Ser-124, and Arg-201 inside the putative translocation pathway and Arg-228 and Asp-382 exposed at the cytoplasmic surface of the protein. The activities of the wild-type and mutant proteins have been analyzed using expression in *E. coli* and radioactive P_i transport assays and compared with bacterial cells carrying an empty plasmid. The results from P_i- and Na^+-dependent kinetics indicate the following: (i) Arg-120 and Arg-201 may be important for binding and translocation of the substrate; (ii) Ser-124 may function as a transient binding site for Na^+ ions in close proximity to the periplasmic side; (iii) Arg-228 and Asp-382 may participate in interactions associated with protein conformational changes required for full transport activity. Functional characterization of ANTR1 should provide useful insights into the function of other plant and mammalian SLC17 homologous transporters.

Solute and metabolite transport proteins are essential for many physiological processes in an organism such as growth, nutrition, cell homeostasis, signal transduction, and stress responses. In plant chloroplasts, where photosynthesis takes place, the vast majority of characterized transporters are from the inner envelope membrane, whereas only a few have been identified in the thylakoid membrane (for recent reviews, see refs *1*−*3*).

Inorganic phosphate (P_i) is a solute essential for ATP synthesis during the photosynthetic light reactions, and it is supplied in the chloroplast stroma by several types of envelope transporters (for reviews, see refs *4* and *5*). The first thylakoid P_i transporter has been recently identified in *Arabidopsis thaliana* (*Arabidopsis*). This is anion transporter 1 (ANTR1)[1], which has been initially localized to the chloroplast using labeling with the green fluorescent protein and fluorescent microscopy and most recently to the thylakoid membrane using peptide-specific antibodies (*6*, *7*). Its expression is restricted to photosynthetic tissues and follows a circadian rhythm (*8*, *9*). ANTR1 has been characterized as a Na^+-dependent P_i transporter when expressed in *Escherichia coli* (*E. coli*) and as a H^+-dependent P_i transporter when expressed in yeast (*7*, *8*). Therefore, this protein is also known as PHT4;1 (*8*). It is presumed to function as a symporter, but the nature of the cotransported ion in *Arabidopsis* chloroplasts has not yet been investigated. As for a role *in planta*, it has been proposed to export P_i produced during nucleotide metabolism in the thylakoid lumen (*10*) to the chloroplast stroma.

The ANTR, *alias* PHT4, family belongs to the ubiquitous major facilitator superfamily (MFS) and consists of six members in *Arabidopsis*, sharing 30−65% sequence identity (*6*). They display 29−34% sequence identity with the mammalian members of the solute carrier 17 (SLC17) family, including sialin, vesicular glutamate transporters (VGLUTs), and Na^+/P_i cotransporters (NPTs) (*6*). Notably, ANTRs selectively transport P_i (*7*, *8*), in contrast to SLC17 members, displaying a broad range of anionic substrates, such as sialic acid, glutamate, organic acids, P_i, and chloride (for a review, see ref *11* and references cited therein).

[†]This work was supported by grants from the Swedish Research Council (to C.S. and B.L.P.), the Swedish Research Council for Environment, Agriculture, and Space Planning (Formas) (to C.S.), Linköping University (to C.S. and B.P.), and the Helge Ax:son Johnson Foundation (to P.M.K.).

*To whom correspondence should be sent. Telephone: 46 13 282681. Fax: 46 13 281399. E-mail: corsp@ifm.liu.se.

[1]Abbreviations: ANTR1, anion transporter 1; GlpT, glycerol 3-phosphate/phosphate antiporter; IPTG, isopropyl 1-thio-β-D-galactopyranoside; MFS, major facilitator superfamily; MSA, multiple sequence alignment; P_i, inorganic phosphate; SLC, solute carrier; TM, transmembrane segment; VGLUT, vesicular glutamate transporter; WT, wild-type ANTR1.

 Published on Web 06/22/2010

Several prokaryotic MFS transporters, namely, glycerol 3-phosphate/phosphate antiporter (GlpT), lactose/H^+ symporter (LacY), multidrug resistance protein D (EmrD), all three from *E. coli*, and the oxalate/formate antiporter (OxlT) from *Oxalobacter formigenes*, have been crystallized (*12*−*15*). GlpT, LacY, and OxlT three-dimensional (3-D) structures have been obtained in the cytoplasmic-facing orientation, whereas the EmrD structure is available in an intermediate conformation. The current view is that the structure of most MFS members consists of two six-helix bundles connected by a large loop and with both termini facing the cytoplasm. A single substrate-binding site, which has alternating access to either side of the membrane (rocker switch), has been proposed to mediate solute transport by GlpT and LacY (*16*, *17*). Among SLC17 proteins, this topology has been validated for VGLUT2, using antibodies against various epitopes (*18*). It is likely that many other structural and functional features of GlpT and LacY are valid for SLC17 members.

In this study we have identified five potentially important amino acids for the function of *Arabidopsis* ANTR1 in P_i transport, based on multiple sequence alignments (MSAs) with other plant ANTRs and mammalian SLC17 homologues and homology modeling using GlpT as a template. Site-directed mutagenesis combined with activity assays in transformed *E. coli* cells verified the importance of these residues for P_i transport. Our findings may have relevance for elucidation of the mechanism of transport by SLC17-type of transporters.

EXPERIMENTAL PROCEDURES

Site-Directed Mutagenesis and Expression in E. coli. The pTrcHisC plasmid (Invitrogen, U.K.) was used for expressing the His_6-Xpress-ANTR1-FLAG fusion protein in *E. coli* TOP10F′ cells (Invitrogen, U.K.) as previously described (*7*). The mutants were prepared by oligonucleotide-directed amino acid-specific mutagenesis using the Stratagene Quikchange II kit (La Jolla, CA). The oligonucleotides used are listed in Supporting Information Table S1. The PCR products were subcloned into the plasmid containing the wild-type ANTR1 (WT) cDNA and sequenced to verify the substitutions.

Transport Assay. Cells transformed with WT or mutant cDNA as well as control (carrying an empty plasmid) cells were assayed as previously described (*7*). Briefly, cells were precultivated overnight in standard Terrific broth medium, containing 70 mM potassium phosphate buffer (TB, pH 7.5) supplemented with 50 μg/mL ampicillin, and reinoculated to an optical density (A_{600}) of 0.6 in fresh TB medium, supplemented with 50 μg/mL ampicillin and 100 μM isopropyl 1-thio-β-D-galactopyranoside (IPTG) for induction for 4 h at 25 °C. The cells were then harvested by centrifugation, resuspended to an A_{600} of 0.3 in TB medium prepared without the addition of P_i, and starved for 1 h. Cells were harvested by centrifugation and washed with 25 mM Tris−succinate buffer (pH 6.5). P_i uptake was assayed by the addition of 1 μL of [^{32}P]orthophosphate (50 mCi/mmol; 1 mCi = 37 MBq; Perkin-Elmer, USA) to a final concentration of 100 μM in 20 μL aliquots, each containing 2 mg (wet weight) of cells in Tris−succinate buffer (pH 6.5), supplemented with 3% glucose, in the presence of 25 mM NaCl or choline chloride. The suspension was incubated for 3 min at 25 °C. P_i transport was terminated by the addition of 1 mL of ice-cold 25 mM Tris−succinate buffer, pH 6.5, and rapid filtration under vacuum (*7*). After three washes with the same ice-cold buffer, the radioactivity retained on the filter was determined by liquid scintillation spectrometry. Results are the average of two to three independent experiments performed in triplicate ± SD.

For determination of the apparent P_i transport affinity (K_m) and maximal rate (V_{max}), uptake of $^{32}P_i$ was carried out for 3 min using a range of concentrations between 0 and 200 μM in the presence of 25 mM NaCl. For the analysis of Na^+-dependent kinetics, the cells were incubated for 3 min with 100 μM P_i and the indicated concentrations of NaCl (0−25 mM). Osmolarity was kept constant with choline chloride. Results were analyzed using the Michaelis−Menten equation by nonlinear regression (Prism 5, GraphPad software). K_m and V_{max} are means of two to three independent experiments performed in triplicate ± SE.

SDS−PAGE and Western Blotting. To verify expression levels of the WT and mutant FLAG-tagged proteins, *E. coli* cells induced with IPTG for 4 h were harvested by centrifugation. The cells were then resuspended and lysed for 30 min on ice in 20 mM Tris-HCl (pH 7.4), 100 mM NaCl, 2 mM $MgCl_2$, 0.5 mM tris(2-carboxyethyl)phosphine hydrochloride, 1% (w/v) Triton X-100, 1% dodecyl maltoside, protease inhibitor cocktail (Sigma), and 1 mg/mL lysozyme (Sigma), followed by sonication. Thereafter, the cell lysate was incubated for 2 h under gentle agitation at 4 °C, followed by centrifugation for 30 min at 20000*g*, to remove cell debris and vesicles. Equivalent amounts of protein lysate (1 A_{600} unit per lane) were separated in 12% (w/v) polyacrylamide−SDS gels and transferred to PVDF membranes (Millipore, Bedford, MA). Thereafter, the membranes were probed with primary anti-FLAG M2 monoclonal antibodies (Sigma), followed by incubation with secondary anti-mouse horseradish peroxidase-conjugated antibodies and chemiluminescent substrate kit (GE Healthcare, U.K.). To quantify the protein expression levels in various mutants, densitometry analysis of the protein band signals on blots was performed using the ImageJ software (NIH, Bethesda, MD). Where indicated, an ANTR1-specific antibody was also used to verify that the anti-FLAG antibody detected signal is the ANTR1 protein, as previously described (*7*).

Multiple Sequence Alignments. To identify functionally important amino acid residues in the ANTR1 sequence, a conservation analysis was performed based on four different MSAs calculated using MUSCLE (*19*). The first MSA was obtained using the amino acid sequences of the six ANTR members from *Arabidopsis*. The second and third MSAs were obtained from a homology search performed at the ARAMEMNON plant membrane protein database (*20*) with criteria of 36% (7 sequences) and 20% (13 sequences) identity, respectively. The fourth MSA was obtained from a BLAST search at the UniProt database (fragments excluded) with an *E*-value $<10^{-40}$ (42 eukaryotic sequences, including mammalian SLC17 homologues).

Homology Modeling and Substrate Docking. The ANTR1 model was constructed based on the structure of GlpT (PDB ID: 1PW4) (*12*). An initial alignment with the template was performed using ClustalW for amino acid residues 84−512 from ANTR1 and revealed 18% identity. Of the missing 83 residues in the N-terminus, region 1−59 is a transit peptide (*7*). Three other structures were also evaluated as potential templates, displaying the same or lower sequence identity with ANTR1, namely, OxlT (18%), EmrD (17%), and LacY (13%). This information and the fact that GlpT transports P_i determined us to choose it as template for homology modeling of ANTR1.

Next, we have performed a transmembrane helix prediction at the ARAMEMNON database, which applies 17 different prediction methods. Most methods predicted 9−11 transmembrane

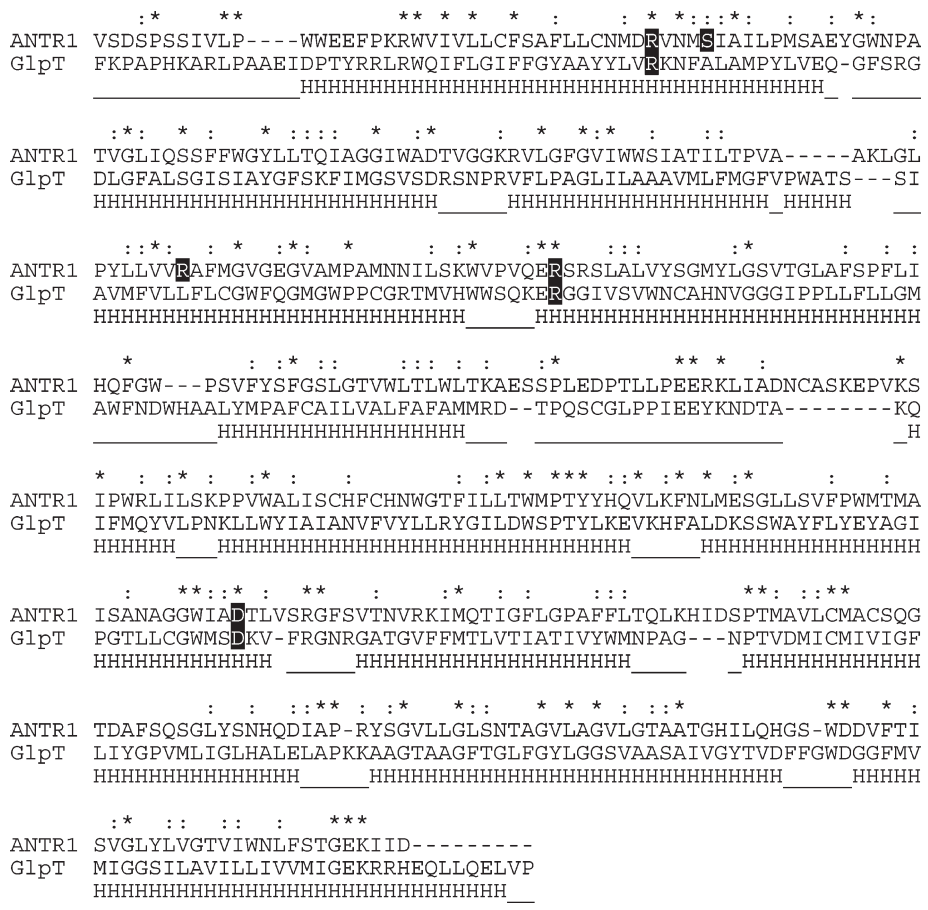

FIGURE 1: Sequence alignment and secondary structure comparison between ANTR1 from *Arabidopsis* and the template protein GlpT from *E. coli*. The sequence alignment was obtained using a combination of transmembrane helix prediction, multiple sequence alignments, and minor manual adjustments. The identical (*), conserved (:), and semiconserved (.) amino acids are indicated above the alignment. The five residues from ANTR1 selected for mutagenesis and functional characterization are highlighted on a dark background. The 12 transmembrane helices (H regions) and connecting loops (—), as detected in the crystal structure of GlpT (*12*), are indicated below the alignment.

segments (TM) for ANTR1. One prediction, however, indicated 12 TMs, the HmmTop_v2 (*21*), which is consistent with the consensus prediction for three other ANTRs at ARAMEMNON database. This also corresponds with the 12 TM topology of crystallized MFS members (including the template) and was therefore used to improve the initial sequence alignment between ANTR1 and GlpT. To improve the quality of regions showing lower conservation in the alignment, such as the large loop between the two six-helix domains, we have performed small adjustments based on the MSA of ANTR1 with the other *Arabidopsis* ANTRs and the one with eukaryotic homologues at the UniProt database. The final pairwise alignment used for homology modeling of ANTR1 is shown in Figure 1.

Three models were created using ICM 3.5 from Molsoft Inc. (*22*), and the model with the lowest energy value and the least number of outliers in the Ramachandran plot was chosen as the final structure. The PROCHECK results (*23*) showed no large errors in this structure, as based on the following: 83.1% of the residues in allowed regions, 13.7% in additional allowed regions, 1.6% in generously allowed regions, and 1.6% in disallowed regions. Conservation analysis was performed using ConSurf (*24*, *25*). Visual analysis and manipulation of the model was done using ICM. The obtained model structure is available at the Protein Model DataBase (*26*) under PMDB ID: PM0076247.

As for the homology modeling, ICM 3.5 was employed for substrate docking. By using the built-in pocket finder, the binding pocket was identified. Here, a ball of a water molecule size was rolled around the protein structure to define its surface; thereafter, pockets with large enough volume and depth were identified. Residues involved in the pocket were defined as those that had any contact with the surface. The pocket we chose for docking prediction is located inside the transportation pathway shown in Figure 2. Even though the binding pocket was quite large, we performed three completely unbiased docking calculations with flexible ligand and side chains in the pocket, while the rest of the protein was treated as rigid. The docking conformation with the lowest total binding energy was treated as the best conformation.

RESULTS

Homology Modeling, Substrate Docking, and Conservation Analysis. The 3-D structure of any member of the *Arabidopsis* P_i transporter (ANTR) family is presently unknown. The crystal structure of GlpT in a cytoplasmic-open conformation (*12*) was chosen as template to model the thylakoid member of this family (ANTR1), as described in Experimental Procedures. The modeled structure consists of two six-TM-containing domains, connected by a large loop and forming a central cavity open toward the cytoplasm (Figure 2A and Supporting Information Figure S1). The TMs forming the cavity are the same as in GlpT, namely, TM1, -2, -4, -5, and the lower part of TM6 from the first domain and TM8, -10, and -11 from the other domain. The diameters of the cavity are the following: 9 Å at the bottom (periplasmic side), 6 Å in the middle, and 5 Å at the entrance

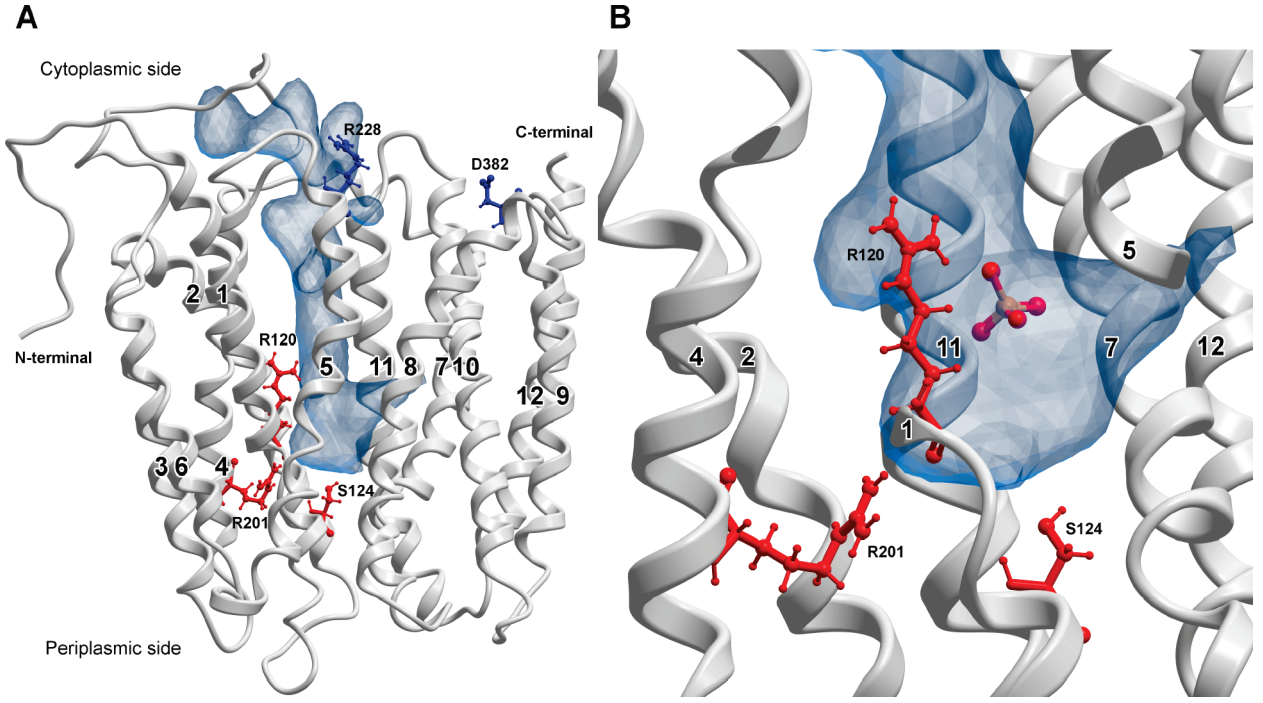

FIGURE 2: Homology model of ANTR1. (A) Ribbon structure of ANTR1 (side view) based on homology modeling using GlpT as a template. The transmembrane segments are labeled 1−12. The main cavity situated between the two domains is shown in blue. The side chains of the five residues selected for site-directed mutagenesis are indicated as follows: Arg-120, Ser-124, and Arg-201 (red); Arg-228 and Asp-382 (blue). (B) Close-up view of the putative phosphate-binding pocket, as determined from docking predictions. The positions of Arg-120, Ser-124, and Arg-201 are shown. The figure was created using ICM Molsoft.

(cytoplasmic side). The sequences of GlpT and ANTR1 are more similar in the TMs forming the cavity than in those outside the cavity (TM3, -7, -9, and -12) (Figure 1). When the model was analyzed using ConSurf, the inner core of the ANTR1 structure was found to be highly conserved (Supporting Information Figure S2), indicating confidence in the pairwise alignment. TM1 contains eight residues that are identical in the two proteins followed by TM11 with six identical residues. Least identity is found in TM5 with only three residues, Glu-227, Arg-228 (mutated in this study), and Gly-242. The main cavity is the putative translocation pathway, expected to contain residues involved in substrate binding and translocation (Figure 2A).

Docking predictions into the putative translocation pathway of ANTR1 were performed for P_i and also for glutamate. The best binding position for P_i was found to be located about 6 Å up from the bottom of the cavity, close to residue Arg-120 (Figure 2B). A distinct location, namely, at the bottom of the cavity, at the level of residue Arg-201, was preferred by the relatively large ligand glutamate (data not shown). Interestingly, a docking study in a GlpT-based homology model of VGLUT1 revealed positioning of the glutamate substrate across the cavity and with two sites of similar binding energy (*27*), one central and one lower in the cavity, in level with Arg residues corresponding to Arg-120 and Arg-201 of ANTR1, respectively. The docking of P_i in VGLUT1 was similar to the one in the present study. The explanation for the discrepancy in positioning of glutamate could be the fact that the bottom of the cavity is 3 Å wider in ANTR1 as compared to the VGLUT1 model.

Four MSAs of ANTR1 with *Arabidopsis* ANTRs, plant homologues at the ARAMEMNON database (>36% and >20% identity) and eukaryotic homologues at the UniProt database (*E*-value $<10^{-40}$) were created. A complete sequence alignment of ANTR1 with homologues found at UniProt database is shown in Supporting Information Figure S3. Using information gained from the docking predictions, position in the structure, and type of amino acid residue, the 25 most conserved residues in all MSAs were classified in four groups, namely, binding/translocation, exposed, closed, and other (Table 1). The side chains of these residues have been highlighted in various colors in the ANTR1 model structure (Supporting Information Figure S4). "Binding/translocation" is a group of three charged or hydrophilic amino acid residues (Arg-120, Ser-124, and Arg-201) located inside the cavity and predicted to be involved in binding and translocation of the substrate and/or coupling ion. "Exposed" group consists of two charged residues, Arg-228 and Asp-382, which are both exposed at the cytoplasmic surface in the modeled conformation and believed not to be directly involved in translocation. "Closed"' includes residues located inside a small cavity at the periplasmic side, which is not open to substrates in the modeled conformation. Finally, the "other" group contains residues that are believed to be solely important for the stability of the protein structure. Seventeen out of the 25 amino acids (68%) are located in TM1, -2, -4, -7, and -8. When mapping them onto the model structure, many were found situated in the cavity, supposed to be the translocation pathway of ANTR1 (Supporting Information Figure S4).

Figure 3 shows an MSA of ANTR1 with selected members of the SLC17 family, all from human except NPT4. We used the rat sequence of NPT4 because the human sequence lacks 77 amino acid residues in TM4 and TM5, as compared to its orthologues and paralogues. Highlighted are the five residues classified as "binding/translocation" and "exposed" in Table 1. These residues are located in TM1, -4, -5, and -8, as based on the alignment with GlpT (Figure 1) and its 3-D structure (*12*). All five residues except Ser-124 were found identical in SLC17 members. Ser-124 residue is replaced with Gly in VGLUTs and with Asn in NPT1. VGLUT1, VGLUT2, and NPT1 have been shown in hetero-

Table 1: Classification of the 25 Most Conserved Residues in ANTR1 Homologues[a]

amino acid residue	ANTR 1−6	ARAMEMNON, >36% identity	ARAMEMNON, >20% identity	UniProt 10^{-40} cutoff	TM no.
binding/ translocation					
R120	:	*	*-1	*-3	1
S124	*	*	*-1		1
R201	*	*	:	*-3	4
exposed					
R228	*	*	*	*-1	5
D382	*	*	*	*	8
closed					
G142	*	*	*	*-2	2
W343	*	*	*		7
P345	*	*	*-1	*-2	7
Y347	*	*	*-1	:-1	7
other					
R102	*	*	:	*-3	1
F148	*	*	*-1		2
Y152	*	*	*-1		2
G160	*	*	*-1	*	2
G205	*	*	*	*-1	4
P213	*-1	*	*		4
W222	*	*	*-1	*-3	4−5
G242	*	*	*	*	5
F263	*	*	*	*	6
G270	*	*		*-2	6
A325	*	*		*-1	7
P366	*	*		*	8
G378	*-1	*	*-1	*-3	8
G439	*	*	*-1	*	10
G463	*-1	*	*-1		11
G475	*-1	*	*		11

[a]Four multiple sequence alignments of ANTR1 with *Arabidopsis* ANTRs, plant homologues at ARAMEMNON database (>36% and >20% identity), and eukaryotic homologues at UniProt database (*E*-value $<10^{-40}$) were created using MUSCLE. The listed amino acid residues are the ones found most conserved in these alignments and are classified in four groups based on their position in the ANTR1 model structure. Asterisks (*) represent an identical amino acid residue, *-1 means identical with one exception, colon (:) means similar properties, and empty box means neither identical nor similar properties. TM, transmembrane segment of ANTR1.

logous system to transport P_i in a Na^+-dependent manner (*28*−*30*) but with 10−100-fold lower affinities as compared to ANTR1. This information and the fact that there are so far no reports on P_i transport by sialin, NPT3, NPT4, and VGLUT3 indicate that a Na^+-dependent P_i transport may not be the primary function for SLC17 members. In GlpT, Ser-124 is replaced with an Ala residue (Figure 1). Since GlpT transports P_i in exchange for glycerol 3-phosphate via a Na^+-independent mechanism, a potential role for Ser-124 in binding of the cotransported Na^+ ion is more likely than one in P_i binding. Arg-120, Arg-228, and Asp-382 were found identical in ANTR1 and GlpT, implying a general role for these residues in the MFS-type of transport mechanism. Residue Arg-201 is only conserved in the SLC17 family and may therefore play a more specific role during transport.

Site-Directed Mutagenesis, Expression, and Activity Characterization of the Wild-Type and Mutant ANTR1 Proteins. On the basis of findings from the homology protein modeling and conservation analysis, we selected five amino acid residues, namely, Arg-120, Ser-124, Arg-201, Arg-228, and Asp-382, for generating site-directed mutant proteins. These mutants were used to study the importance of the selected residues for the function of ANTR1 in P_i transport and its Na^+ dependency. For this purpose, the WT and mutated His_6-Xpress-ANTR1-FLAG constructs were cloned into the pTrcHisC vector and expressed in *E. coli* upon IPTG induction. Western blotting analyses of protein lysate from transformed cells using an anti-FLAG peptide antibody revealed the expression of ANTR1 (M_r of 56 kDa) in WT and mutant cells but not in the control cells (Figure 4 inset). Densitometry analysis revealed a drastic increase in the expression of R228E, R228K, and D382A mutants, ranging between 160% and 200% relative to the WT levels. It is not clear at present the reason for the increased accumulation of these mutants. Nevertheless, for the other mutants, the protein expression levels did not appear to be largely altered, ranging between 80% and 120% relative to the WT levels, indicating that the corresponding mutations did not dramatically perturb the protein structure and stability. The same pattern of protein expression was obtained when using an anti-ANTR1 peptide-specific antibody (data not shown).

The levels of P_i uptake into *E. coli* cells were determined at 3 min in the presence of 25 mM NaCl (Figure 4) and represented relative to the WT levels (100% = 21.6 ± 1.1 nmol of P_i (mg of protein)$^{-1}$). P_i uptake in the control cells under the same conditions yielded 35% of the maximal level accumulated in WT cells and is attributed to the activity by various *E. coli* P_i transporters (*31*). In the presence of choline chloride, WT cells took up 6.9 ± 0.3 nmol of P_i (mg of protein)$^{-1}$, whereas all mutants and control cells displayed uptake levels below 5 nmol of P_i (mg of protein)$^{-1}$ (data not shown).

All mutants had much lower transport activity than protein expression relative to the WT levels. Most mutants displayed reduced transport activity although their expression levels were similar to the WT levels (Figure 4). This indicates that those mutations specifically affected their ability to transport P_i. Hence, to characterize these residues for their role in substrate binding or translocation, we have measured kinetic parameters of the mutants by measuring the initial rates of P_i uptake over a range of P_i concentrations (Supporting Information Figure S5) and subtracting the corresponding control values. As R120E, R201E, R228E, and D382N had very poor activity, these could not be included for the kinetic study. The apparent K_m, V_{max}, and corrected V_{max} values (calculated based on protein expression levels) have been summarized in Table 2.

The estimated K_m for ANTR1 in the present study is in close agreement with the previously reported value (78.7 ± 34 μM (*7*)). However, the V_{max} differed significantly from the previously reported value (161 ± 28 nmol (mg of protein)$^{-1}$ h^{-1}). Since K_m is an intrinsic property of the transporter whereas V_{max} can vary with the protein expression levels and experimental conditions, the results were considered to be reliable and used for evaluation of the mutants. In the last column of Table 2, the ratio between the respective corrected V_{max} and K_m is shown and used to directly compare the efficiency of P_i transport by the various mutated proteins. A value of 4.3 was determined for the WT protein and values ranging between 0.5 and 2.8 in the mutants with measurable activity.

Residue Arg-120 may be found in TM1 inside the cavity, close to the P_i docking position (Figure 1B). Its substitution with Glu reduced P_i uptake at 3 min below the control levels (Figure 3). Its substitution with the smaller Lys resulted in 40% lower P_i uptake activity as compared to the one obtained for the WT. This could

```
                       TM1
                                 R120 S124
ANTR1     PKRWVIVLLCFSAFLLCNMDRVNMSIAILPM
Sialin    SARYNLAILAFFGFFIVYALRVNLSVALVDM
VGLUT1    PRRYIIAIMSGLGFCISFGIRCNLGVAIVSM
VGLUT2    PRRYIIAIMSGLGFCISFGIRCNLGVAIVDM
VGLUT3    PKRYIIAIMSGLGFCISFGIRCNLGVAIVEM
NPT4      SLRYSIAFIAHICNFTLIAQNSIISITMVAM
NPT3      SFRYGLALIMHFSNFTMITQRVSLSIAIIAM
NPT1      SMRYGLSFLVHCCNVIITAQRACLNLTMVVM
          . *: : ::           .  :.:::: *

                       TM4                               TM5
             R201                        R228
ANTR1     LLVVRAFMGVGEGVAMPAMNNILSKW … ERSRSLALVYSGMYLGSVTGLAFSPF
Sialin    LIVLRALEGLGEGVTFPAMHAMWSSW … ERSKLLSISYAGAQLGTVISLPLSGI
VGLUT1    VIFVRILQGLVEGVTYPACHGIWSKW … ERSRLATTAFCGSYAGAVVAMPLAGV
VGLUT2    VIFVRILQGLVEGVTYPACHGIWSKW … ERSRLATTSFCGSYAGAVIAMPLAGI
VGLUT3    VMCVRILQGLVEGVTYPACHGMWSKW … ERSRLATTSFCGSYAGAVVAMPLAGV
NPT4      VIMVRTVQGMAQGMAWTGQFTIWAKW … ERSKLTTIAGSGSAFGSFIILCVGGL
NPT3      VVVCRAVQGAAQGIVATAQFEIYVKW … ERGRLTSMSTSGFLLGPFIVLLVTGV
NPT1      LLATRAVQGLTQGAGYGGQFALWQKW … ERSRLCSIAMSGMILGIFAVLLVGGI
          ::  * . *  :*    .   :  .*   **..  :    .*    *  .  :  .  .

                       TM8
                                D382
ANTR1     MESGLLSVFPWMTMAISANAGGWIADT
Sialin    QENGFLSSLPYLGSWLCMILSGQAADN
VGLUT1    SKVGLVSALPHLVMTIIVPIGGQIADF
VGLUT2    SKVGMLSAVPHLVMTIIVPIGGQIADF
VGLUT3    SKVGLLSAVPHMVMTIVVPIGGQLADY
NPT4      RDSGVLSSLPFIAAASCTILGGQLADF
NPT3      KENGFLSSLPYLFAWICGNLAGQLSDF
NPT1      RDNGLLSSLPFFVAWVIGILGGLLADF
           . *.:* .* :         .*  :*
```

Figure 3: Conservation of mutated residues in ANTR1 and mammalian SLC17 homologues. The amino acid sequences of *Arabidopsis* ANTR1 (UniProt O82390), sialin from human (Q9NRA2), vesicular glutamate transporters VGLUT1−3 from human (Q9P2U7, Q9P2U8, Q8NDX2), and Na^+/P_i cotransporters NPT1 and NPT3 from human (Q14916 and O00624) and NPT4 from rat (Q8CJH9) were aligned using MUSCLE. The five mutated residues are indicated in dark boxes. Conservation is marked in ClustalX style, where asterisks (*) indicate an identical residue, colon (:) represents a similar (conserved) amino acid property, and period (.) corresponds to a semiconserved residue.

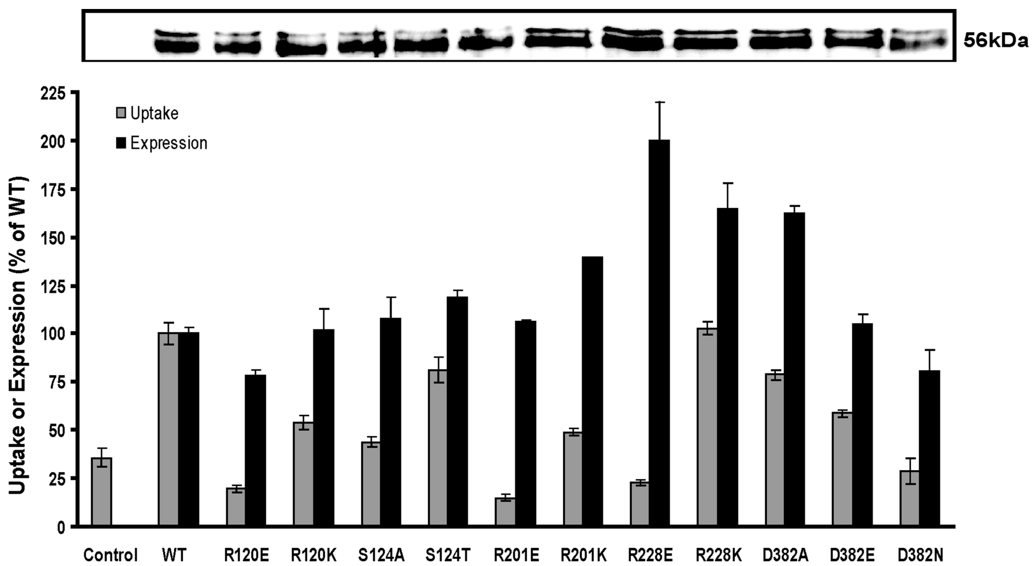

Figure 4: Comparative effects of site-directed mutations on P_i uptake and protein expression levels. The transport activity and ANTR1 protein abundance were measured in *E. coli* cells transformed with an empty vector (control) and cells expressing the wild-type ANTR1 (WT) or mutant protein and are shown as a percentage of the WT levels. The transport activity of 100 μM $^{32}P_i$ was measured for 3 min in 25 mM Tris−succinate (pH 6.5) in the presence of 25 mM NaCl. Protein expression was determined by quantification of the ANTR1 Western blots. The bars are means ± SD. Inset: Representative Western blot of protein lysate (1 A_{600} unit per lane) from *E. coli* cells with an anti-FLAG peptide antibody. The loaded samples correspond to the strains in the plot. The equal loading of the proteins in each well of the gel was visually monitored by Coomassie staining of duplicate gels (data not shown). The mass of ANTR1 is approximately 56 kDa, indicated to the right of the blot.

be explained by the 2-fold increase in K_m, resulting in a nearly 3-fold decrease in transport efficiency of the mutant (Table 2). These results indicate that Arg-120 may be an important residue for P_i binding and associated conformational changes.

Ser-124 may be located in TM1 at the bottom of the cavity in the cytoplasmic-open conformation (Figure 1). This residue could function as a transient binding site for P_i and/or coupling ions. Its substitution with Ala, which is nonpolar and lacks an

Table 2: Apparent Kinetic Parameters for P_i Transport of Wild-Type ANTR1 and Mutants[a]

mutation	K_m (μM)	V_{max} (nmol (mg of protein)$^{-1}$ h^{-1})	corrected V_{max}[b] (nmol (mg of protein)$^{-1}$ h^{-1})	corrected V_{max}/K_m (nmol (mg of protein)$^{-1}$ h^{-1} μM^{-1})
WT	77.1 ± 20.7	329.0 ± 35.8		4.3
R120K	161.0 ± 57.9	255.0 ± 47.7	250.0	1.6
S124A	44.8 ± 16.5	50.9 ± 6.2	47.1	1.1
S124T	109.0 ± 40.9	303.0 ± 51.9	254.6	2.4
R201K	214.0 ± 75.5	141.0 ± 28.2	100.7	0.5
R228K	103.0 ± 28.0	453.0 ± 55.1	274.5	2.5
D382A	57.2 ± 9.7	253.0 ± 15.7	156.2	2.8
D382E	46.2 ± 17.9	101.0 ± 13.2	96.2	2.1

[a]The uptake of various concentrations of $^{32}P_i$ was carried out for 3 min in 25 mM Tris−succinate buffer (pH 6.5) containing 25 mM NaCl. The values obtained for wild-type ANTR1 (WT) and mutant cells were subtracted by those in the control cells. Apparent maximum velocity (V_{max}) and K_m values were determined by fitting the data to the Michaelis−Menten equation using the nonlinear regression program Prism 5. V_{max}/K_m ratio is a measure of transport efficiency. Data shown are means of two to three experiments ± SE. [b]V_{max} was adjusted to the protein expression levels.

Table 3: Apparent Na^+-Dependent Kinetic Parameters for P_i Transport of Wild-Type ANTR1 and Mutants[a]

mutation	K_m (mM)	V_{max} (nmol (mg of protein)$^{-1}$ h^{-1})	corrected V_{max}[b] (nmol (mg of protein)$^{-1}$ h^{-1})
WT	0.84 ± 0.38	267.0 ± 26.5	
R120K	1.48 ± 0.90	128.0 ± 18.6	125.5
S124A	0.27 ± 0.30	67.0 ± 10.9	62.0
S124T	0.88 ± 0.58	265.0 ± 38.1	222.7
R201K	2.29 ± 0.83	176.5 ± 16.7	126.1
R228K	1.99 ± 0.83	365.0 ± 38.6	221.2
D382A	0.49 ± 0.51	193.0 ± 37.6	119.1
D382E	0.73 ± 0.53	139.0 ± 21.2	132.4

[a]The uptake of $^{32}P_i$ (100 μM) was carried out for 3 min in 25 mM Tris−succinate buffer (pH 6.5) in the presence of various concentrations of NaCl. Choline chloride was added to preserve osmolarity. The obtained uptake values for wild-type ANTR1 (WT) and mutant cells were subtracted by those in the control cells. Apparent maximum velocity (V_{max}) and K_m values were determined by fitting the data to the Michaelis−Menten equation using the nonlinear regression program Prism 5. Data shown are means of two to three experiments ± SE. [b]V_{max} was adjusted to the protein expression levels.

OH group at the β-carbon, resulted in reduction of the P_i uptake down to the control levels (Figure 4). A reduction by 7-fold was determined for the corrected V_{max} value, resulting in a 4-fold decrease in transport efficiency (Table 2). These results indicate a critical role of this residue in the conformational changes associated with the translocation rather than in binding of the substrate itself.

The S124T mutant, preserving the OH group at the β-carbon, displayed only slightly lower uptake levels than WT cells (Figure 4). K_m increased while the corrected V_{max} decreased by 1.5-fold (Table 2). The data obtained for S124A and S124T show that the presence of an OH group at the β-carbon is necessary for P_i transport activity. Furthermore, the data also indicate that Ser and Thr may have slightly different impact on the helix packing since the S124T mutant displayed nearly 2-fold lower transport efficiency for P_i.

Residue Arg-201 may be found in TM4 inside the cavity, where it may participate in P_i binding. The R201E mutant displayed levels of P_i uptake at 3 min below the control levels (Figure 4). The Arg-201 substitution with Lys resulted in 45% lower uptake as compared to WT and had drastic effects on the transport kinetics, since K_m increased whereas V_{max} decreased by 3-fold. Among all mutants used in this study, R201K was the one with the lowest transport efficiency, i.e., nearly 9-fold lower than WT, confirming the crucial importance of this residue for P_i binding and translocation.

The highly conserved residue Arg-228 may be located in TM5 at the outer surface of the protein, far from the predicted P_i binding site. Its substitution with Glu resulted in a drastic reduction of uptake at 3 min below the control levels, as in the case of R120E and R201E mutations (Figure 4). Lys substitution of Arg-228 resulted in slightly higher uptake levels at 3 min as compared to WT, consistent with its higher relative expression levels (Figure 4). Only a weak impact on the kinetic parameters and nearly 2-fold lower P_i transport efficiency were observed for this mutation. Thus, although further experimentation may be required, Arg-228 appears to be important for a full P_i transport activity.

Residue Asp-382, located at the exit of TM8, may be involved in interaction with positively charged residues and/or with coupling ions. However, substitution of this residue with Ala did not affect the uptake at 3 min, while it only slightly decreased K_m and reduced by 2-fold V_{max}, without dramatically changing the transport efficiency (V_{max}/K_m). Its substitution with Glu lowered by 2-fold the transport efficiency, mainly due to more than 3-fold reduction in V_{max}. The uptake at 3 min was reduced by 45% in the D382E and below the control levels in the D382N mutant. These data indicate a weak participation of Asp-382 in interactions involved in protein conformational changes required for transport.

To test the possibility that the observed changes in V_{max} are due to an effect of mutations on the binding of coupling ions, we have performed uptake of 100 μM P_i in the presence of various concentrations of NaCl (0−25 mM) in those mutant strains, which show detectable levels of activity (Supporting Information Figure S6). The apparent kinetic parameters for Na^+ were determined after subtracting the corresponding control values. The K_m value for Na^+ of WT ANTR1 (Table 3) is in close agreement with the previously reported value (1.17 ± 0.36 μM (*7*)). As observed in the case of P_i kinetics, the V_{max} for Na^+ differs significantly from the previously reported value (99.15 ± 5.17 nmol (mg of protein)$^{-1}$ h^{-1}), most likely due to changes in the protein expression levels and experimental conditions.

Variations in the K_m (Na^+) and V_{max} values with respect to WT were observed in cells expressing mutants of the Arg-120 and Arg-201 residues, namely, 2−2.5-fold increase in K_m and corresponding decrease in corrected V_{max} values (Table 3). However, the observed effect on Na^+ kinetics in the two mutants most likely reflects the direct effect of mutation on P_i binding and

translocation. Notably, substitution of Ser-124 with Ala lowered V_{max} by over 4-fold and impaired the Na^+ dependency, whereas substitution with Thr did not affect either of the kinetic parameters, emphasizing the importance of the hydroxyl group of this residue for Na^+ binding. The mutant R228K displayed over 2-fold increase in K_m and only slight effects on V_{max}, strengthening that this residue is not directly involved in binding either of the substrate or of the coupling ions. Asp-382 substitutions to Ala or Glu showed only slight effects on K_m (Na^+) and over 2-fold reduction in V_{max} as compared to WT. The kinetic data indicate a participation of Arg-228 and Asp-382 residues in the conformational changes associated with the translocation and required for full activity. Taken together, the results of Na^+ kinetic experiments indicate that among the mutated residues, Ser-124 may be involved in Na^+ binding and translocation during P_i transport.

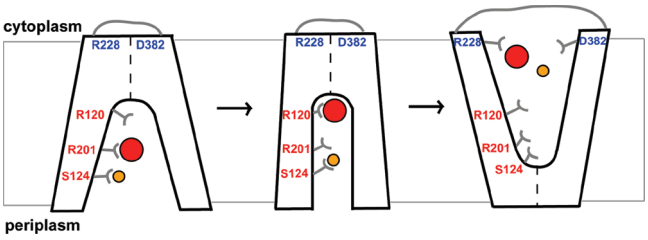

FIGURE 5: Schematic diagram of substrate binding and alternating-access mechanism of ANTR1. Like MFS transporters, the conformational cycle of ANTR1 may feature a state open to the periplasmic side, an intermediate state with the substrate and coupling ion bound, and one state open to the cytoplasmic side of the membrane. The diagram shows the proposed roles for five residues analyzed in this study: Arg-120, Ser-124, Arg-201, Arg-228, and Asp-382. The P_i substrate is represented by a red disk and Na^+ ion by a yellow disk.

DISCUSSION

The structures of four MFS transporters have been solved (*12*−*15*), and despite the low amino acid sequence identity, they were found to be highly similar. This led to the hypothesis that all MFS members share an overall similar structure, regardless of the broad substrate specificity. Among the four crystal structures available, the one of GlpT was chosen as a template for homology modeling of thylakoid P_i transporter (ANTR1) from *Arabidopsis*, as it has been used for modeling of other prokaryotic and eukaryotic MFS transporters (for a recent review, see ref *32*). Moreover, GlpT produced the best alignment scores among the tested structures and is known to function as a glycerol 3-phosphate/P_i antiporter.

To our knowledge, there is no similar study to the present one for direct identification of key residues in P_i transporters from plants or animals. So far, only a homologous structure of a H^+-coupled P_i transporter from *Saccharomyces cerevisiae* (Pho84) has been reported (*33*), and recently homology modeling has been used to model H^+-coupled P_i transporters of type 1 (PHT1) from *Medicago truncatula* to identify amino acid residues responsible for differences in the affinity between the members of this family (*34*).

Integrating information from a combination of structural modeling, MSAs, and substrate docking, we have identified and selected for mutagenesis five charged or hydrophilic residues, which are highly conserved in plant ANTRs, mammalian SLC17 members, and even MFS members (GlpT), namely, Arg-120, Ser-124, Arg-201, Arg-228, and Asp-382. The mutated variants of ANTR1 were thereafter expressed and functionally characterized in *E. coli*. Immunoblot analysis confirmed that each of the mutant proteins was expressed although in variable amounts (Figure 4 inset). Data from Figure 4 clearly show that substitution of the three Args (120, 201, and 228) for Glu residue and of Asp-382 for Asn residue resulted in an inactive ANTR1 transporter. Notably, these mutations may affect the general physiology of the bacterial cells via an unknown mechanism, since they result in transport activities even lower than the control cells. All other mutants had sufficient activity to allow measurement of kinetic parameters, attesting that the mutated proteins were functional.

The kinetic characterization of the mutants revealed interesting insights into the roles of each of the five residues in the function of ANTR1 in P_i transport, which have been schematically illustrated in Figure 5. Based on P_i-dependent kinetics, Arg-201 was found to be the most critical residue for substrate binding and translocation. For the Na^+ dependency of the transport, Ser-124 was found to be a key residue, which may function as a transient binding site for Na^+ ions. Residue Arg-120 was found to play an important role in P_i binding and associated conformational changes. Finally, Arg-228 and Asp-382 may participate in interactions allowing conformational changes to occur at the cytoplasmic surface of the transporter. On the basis of the conservation analysis of these residues (Table 1), our findings may have relevance for the mechanism of transport by plant and mammalian ANTR1 homologues. Particularly, residue Arg-201 is fully conserved among all of these homologues, whereas Ser-124 is fully conserved only among plant homologues at the ARAMEMNON database. As compared to those two residues, Arg-120, Arg-22, and Asp-382 are fully conserved even in GlpT (Figure 1), and therefore our findings may have implications for the general MFS type of transport mechanism.

In previous studies, Arg-45 in GlpT, corresponding to Arg-120 in ANTR1, has been demonstrated using mutagenesis as a key residue for binding of either P_i or anionic phosphoryl group of glyceraldehyde 3-phosphate (*35*). Nevertheless, the corresponding residue in the SLC17 member VGLUT2 (Arg-88) was not found to be critical for glutamate transport (*36*). The same report has found instead the residue corresponding to Arg-201 in ANTR1 to be essential for glutamate transport, whereas neither of the two Arg residues were found to be important for P_i transport by VGLUT2. The results obtained in the present study clearly demonstrate the importance of Arg-120 and Arg-201 for P_i transport by ANTR1. The fact that Arg-201 is fully conserved in the SLC17 family implies that this residue may be important for binding of both organic and inorganic anionic substrates. For comparison, the His-128 residue shown to be essential for glutamate transport by VGLUT2 (*36*) is not conserved in ANTR1 and also neither in human NTPs nor in sialin and may therefore be specific for glutamate binding/transport. The docking predictions performed for ANTR1 indicated a distinct binding position for P_i and glutamate in the transportation cavity, at the level of Arg-120 and Arg-201, respectively. The Arg-201 residue may only be a transient binding site for P_i in ANTR1, to attract it inside the cavity (Figure 5), since docking at this position was found to be less favorable than for Arg-120. In our previous biochemical characterization of ANTR1, glutamate could compete for the P_i transport (by 50%); however, no glutamate transport activity could be detected (*7*). Those data could now be explained based on the findings of the docking predictions and biochemical analysis performed in the present study, indicating that Arg-201, which is close to the best docking position of

glutamate, may at the same time be important for P_i transient binding and transport. For comparison, the two positions corresponding to Arg-120 and Arg-201 were found to be energetically similar when glutamate substrate was docked into the VGLUT1 model (*27*). Those predictions and previous biochemical studies (*36*) may support the hypothesis that both residues are stable binding sites for glutamate in VGLUTs.

It has been proposed that either Na^+ or H^+ ions are required for transport of P_i by ANTR1 (*7*, *8*). For LacY, a His residue inside the cavity has been proposed to bind the H^+ ions involved in cotransport (*16*). There are only three His residues on the inside of the ANTR1 protein, located opposite to Arg-120 and Arg-201, namely, His-330, His-333, and His-444. None of them is fully conserved among plant ANTRs. Moreover, they do not have direct access to the cavity, even though the side chains are pointing in the right direction. If any of the ANTRs would be a H^+-coupled transporter, dramatic changes must occur to expose any of these histidines, or there must be some other types of residues involved in H^+ binding/transport. Nevertheless, all six members of the ANTR family have been characterized as H^+-dependent P_i transporters when expressed in yeast (*8*). This implies that there must be some other types of residues involved in H^+ cotransport, which may be present among the ones listed in Table 1.

Na^+/solute cotransporters require mainly OH-containing groups (Ser, Thr) but also acidic residues (Glu, Asp) for binding and translocation of the coupling ion, as revealed in the recent crystal structure of LeuTA (*37*). The target for Na^+ binding in this study has been Ser-124. This residue is located at the bottom of the cavity in the cytoplasmic-open conformation (Figure 5). It may be a fast operating gateway by short-lived binding of Na^+ ions. Its closest partner in coordinating the Na^+ ions may be Thr-342 residue from the other domain, at a distance of around 4 Å between OH groups, in the modeled ANTR1 structure.

Arg-228 and Asp-382 are actually the most conserved residues among the five studied ones (Table 1), even though they both may reside close to the cytoplasmic surface, and are far away from the substrate-docking site (Figure 5). The R228E and D382N mutants completely lost the transport activity, whereas a partial loss was obtained in R228K, D382E, and D382A mutants. Although it is not clear at the present stage which type of interactions the two residues make, we suggest that their presence at positions 228 and 382, respectively, is required for full activity. An attractive possibility could be that, due to its basic properties, Arg-228 may participate in transient binding of anionic substrates, such as P_i, on the way out from the cavity into the cytoplasm. Notably, ANTR1 amino acid sequence was shown to contain a seven-residue consensus pattern for the MFS anion:cation symporter family, which includes Arg-228 (*6*, *7*, *38*). Conserved cationic residues such as Arg are also part of other MFS family specific consensus sequences (*38*) and could be important for both structural and functional aspects. A relevant question is why among all studied mutants R228E accumulates in the largest amounts as compared to WT (200%) and is inactive (Figure 4). We tempt to speculate that this mutant is partially folded/misfolded for two possible reasons: When close to the cytoplasmic surface, the positively charged side chains may interact with negatively charged phosphate groups at the lipid bilayer surface or may promote packing of TMs by H-bond formation with neighboring residues, resulting in proper folding and/or insertion of the protein (*39*, *40*).

It is important to consider the fact that the crystal structure of GlpT was obtained in the absence of a substrate, revealing a cytoplasmic-open conformation and with a tightly closed periplasmic side (*12*). In the case of LacY, the same conformation was obtained in the presence of a lactose homologue, β-D-galactopyranosyl 1-thio-β-D-galactopyranoside (*13*). Recently, it has been shown that, in the presence of the native substrate, LacY adopts the periplasmic-open conformation, indicating that the structure of the binding pocket undergoes a rocker-switch conformational change (*41*). Experimental evidence for as much as 15−17 Å large periplasmic-open cavity has been reported for LacY (*42*), which implies that the cavity can be closed at the cytoplasmic side. In order for transformed *E. coli* cells to take up P_i via ANTR1, a hydrophilic pathway must open at the periplasmic side to allow access of P_i to the binding site. Since P_i transport shows strong dependency on Na^+ concentration (Supporting Information Figure S6), initial or simultaneous Na^+ binding may be required. To explain the effects of various substitutions on P_i and Na^+ kinetics (Tables 2 and 3), we propose that binding of Na^+ ions by Ser-124 may allow opening at the periplasmic side and access of P_i inside the cavity (Figure 5). The positively charged Arg-201 may attract P_i in the cavity before reaching its binding position, close to Arg-120, in the intermediate conformation. This results in the structural change leading to the cytoplasmic-open conformation and subsequent release of the substrate and coupling ion. We suggest that Arg-228 and Asp-382 participate in interactions at the cytoplasmic side, possibly by attracting the substrate out from the cavity, preparing the structure for the periplasmic-open conformation and a new transport cycle. Arg-228 may also be important for proper insertion/folding of the protein in the membrane.

The present study based on *Arabidopsis* ANTR1 provides the first data on the 3-D molecular interactions of a P_i transporter with its substrate and the coupling ion. The homology model can be used to target other key amino acids responsible for P_i binding, membrane interaction, and interactions with other components. The functionally important residues in ANTR1 may help to understand the mechanism of solute transport by SLC17 homologues and could even be expanded to other MFS members. *In vivo* inhibitors should offer possibility to mimic the phenotype of plant ANTR1 mutants.

ACKNOWLEDGMENT

The full-length RAFL09-06-K07 cDNA clone was provided by RIKEN BioResource Center (Japan).

SUPPORTING INFORMATION AVAILABLE

Table S1 and Figures S1−S6 as described in the text. This material is available free of charge via the Internet at http://pubs.acs.org.

REFERENCES

1. Block, M. A., Douce, R., Joyard, J, and Rolland, N. (2007) Chloroplast envelope membranes: a dynamic interface between plastids and the cytosol. *Photosynth. Res. 92*, 225–244.
2. Linka, M., and Weber, A.P. M. (2010) Intracellular metabolite transporters in plants. *Mol. Plant 3*, 21–53.
3. Spetea, C., and Schoefs, B. (2010) Solute transporters in plant thylakoid membranes—key players during photosynthesis and stress. *Comm. Integr. Biol. 3*, 122–129.
4. Flugge, U. I. (1999) Phosphate translocators in plastids. *Annu. Rev. Plant Physiol. Plant Mol. Biol. 50*, 27–45.

5. Weber, A. P., Schwacke, R., and Flügge, U. I. (2005) Solute transporters of the plastid envelope membrane. *Annu. Rev. Plant Biol. 56*, 133–164.
6. Roth, C., Menzel, G., Petétot, J. M., Rochat-Hacker, S., and Poirier, Y. (2004) Characterization of a protein of the plastid inner envelope having homology to animal inorganic phosphate, chloride and organic-anion transporters. *Planta 218*, 406–416.
7. Pavón, L. R., Lundh, F., Lundin, B., Mishra, A., Persson, B. L., and Spetea, C. (2008) Arabidopsis ANTR1 is a thylakoid Na^+-dependent phosphate transporter: functional characterization in *Escherichia coli*. *J. Biol. Chem. 283*, 13520–13527.
8. Guo, B., Jin, Y., Wussler, C., Blancaflor, E. B., Motes, C. M., and Versaw, W. K. (2008) Functional analysis of the *Arabidopsis* PHT4 family of intracellular phosphate transporters. *New Phytol. 177*, 889–898.
9. Guo, B., Irigoyen, S., Fowler, T. B., and Versaw, W. K. (2008) Differential expression and phylogenetic analysis suggest specialization of plastid-localized members of the PHT4 phosphate transporter family for photosynthetic and heterotrophic tissues. *Plant Signal. Behavior 3*, 1–7.
10. Spetea, C., Hundal, T., Lundin, B., Heddad, M., Adamska, I., and Andersson, B. (2004) Multiple evidence for nucleotide metabolism in the chloroplast thylakoid lumen. *Proc. Natl. Acad. Sci. U.S.A. 101*, 1409–1414.
11. Reimer, R. J., and Edwards, R. H. (2004) Organic anion transport is the primary function of the SLC17/type I phosphate transporter family. *Pfluegers Arch. 447*, 629–635.
12. Huang, Y., Lemieux, M. J., Song, J., Auer, M., and Wang, D. N. (2003) Structure and mechanism of the glycerol-3-phosphate transporter from *Escherichia coli*. *Science 301*, 616–20.
13. Abramson, J., Smirnova, I., Kasho, V., Verner, G., Kaback, H. R., and Iwata, S. (2003) Structure and mechanism of the lactose permease of *Escherichia coli*. *Science 301*, 610–615.
14. Yin, Y., He, X., Szewczyk, P., Nguyen, T., and Chang, G. (2006) Structure of the multidrug transporter EmrD from *Escherichia coli*. *Science 312*, 741–744.
15. Hirai, T., Heymann, J. A., Shi, D., Sarker, R., Maloney, P. C., and Subramaniam, S. (2002) Three-dimensional structure of a bacterial oxalate transporter. *Nat. Struct. Biol. 9*, 597–600.
16. Guan, L., and Kaback, H. R. (2006) Lessons from lactose permease. *Annu. Rev. Biophys. Biomol. Struct. 35*, 67–91.
17. Law, C. J., Maloney, P. C., and Wang, D. N. (2008) Ins and outs of major facilitator superfamily antiporters. *Annu. Rev. Microbiol. 62*, 289–305.
18. Jung, S. K., Morimoto, R., Otsuka, M., and Omote, H. (2006) Transmembrane topology of vesicular glutamate transporter 2. *Biol. Pharm. Bull. 29*, 547–549.
19. Edgar, R. C. (2004) MUSCLE: multiple sequence alignment with high accuracy and high throughput. *Nucleic Acids Res. 32*, 1792–1797.
20. Van der Graaff, E., Fischer, K., Catoni, E., Desimone, M., Frommer, W. B., Flügge, U. I., and Kunze, R. (2003) ARAMEMNON, a novel database for *Arabidopsis* integral membrane proteins. *Plant Physiol. 131*, 16–26.
21. Tusnády, G. E., and Simon, I. (2001) The HMMTOP transmembrane topology prediction server. *Bioinformatics 17*, 849–850.
22. Abagyan, R., and Totrov, M. (1994) Biased probability Monte Carlo conformational searches and electrostatic calculations for peptides and proteins. *J. Mol. Biol. 235*, 983–1002.
23. Laskowski, R. A., MacArthur, M. W, Moss, D. S, and Thornton, J. M (1993) PROCHECK: a program to check the stereochemical quality of protein structures. *J. Appl. Crystallogr. 26*, 283–291.
24. Glaser, F., Pupko, T., Paz, I., Bell, R. E., Bechor, D., Martz, E., and Ben-Tal, N. (2003) ConSurf: identification of functional regions in proteins by surface-mapping of phylogenetic information. *Bioinformatics 19*, 163–164.
25. Landau, M., Mayrose, I., Rosenberg, Y., Glaser, F., Martz, E., Pupko, T., and Ben-Tal, N. (2005) ConSurf 2005: the projection of evolutionary conservation scores of residues on protein structures. *Nucleic Acids Res. 33*, W299–W302.
26. Castrignanò, T., De Meo, P. D., Cozzetto, D., Talamo, I. G., and Tramontano, A. (2006) The PMDB protein model database. *Nucleic Acids Res. 34*, D306–309.
27. Almqvist, J., Huang, Y., Laaksonen, A., Wang, D. N., and Hovmöller, S. (2007) Docking and homology modeling explain inhibition of the human vesicular glutamate transporters. *Protein Sci. 16*, 1819–1829.
28. Ni, B., Rosteck, P. R., Nadi, N. S., and Paul, S. M. (1994) Cloning and expression of a cDNA encoding a brain-specific Na(+)-dependent inorganic phosphate cotransporter. *Proc. Natl. Acad. Sci. U.S.A. 91*, 5607–5611.
29. Miyamoto, K., Tatsumi, S., Sonoda, T., Yamamoto, H., Minami, H., Taketani, Y., and Takeda, E. (1995) Cloning and functional expression of a Na(+)-dependent phosphate co-transporter from human kidney: cDNA cloning and functional expression. *Biochem. J. 1305*, 81–85.
30. Aihara, Y., Mashima, H., Onda, H., Hisano, S., Kasuya, H., Hori, T., Yamada, S., Tomura, H., Yamada, Y., Inoue, I., Kojima, I., and Takeda, J. (2000) Molecular cloning of a novel brain-type Na(+)-dependent inorganic phosphate cotransporter. *J. Neurochem. 74*, 2622–2625.
31. Harris, R. M., Webb, D. C., Howitt, S. M., and Cox, G. B. (2001) Characterization of PitA and PitB from *Escherichia coli*. *J. Bacteriol. 183*, 5008–5014.
32. Lemieux, M. J. (2007) Eukaryotic major facilitator superfamily transporter modeling based on the prokaryotic GlpT crystal structure. *Mol. Membr. Bio.l 24*, 333–341.
33. Lagerstedt, J. O., Voss, J. C., Wieslander, A., and Persson, B. L. (2004) Structural modeling of dual-affinity purified Pho84 phosphate transporter. *FEBS Lett. 578*, 262–268.
34. Liu, J., Versaw, W. K., Pumplin, N., Gomez, S. K., Blaylock, L. A., and Harrison, M. J. (2008) Closely related members of the *Medicago truncatula* PHT1 phosphate transporter gene family encode phosphate transporters with distinct biochemical activities. *J. Biol. Chem. 283*, 24673–24681.
35. Law, C. J., Enkavi, G., Wang, D. N., and Tajkhorshid, E. (2009) Structural basis of substrate selectivity in the glycerol-3-phosphate: phosphate antiporter GlpT. *Biophys. J. 97*, 1346–1353.
36. Juge, N., Yoshida, Y., Yatsushiro, S., Omote, H., and Moriyama, Y. (2006) Vesicular glutamate transporter contains two independent transport machineries. *J. Biol. Chem. 281*, 39499–39506.
37. Yamashita, A., Singh, S. K., Kawate, T., Jin, Y., and Gouaux, E. (2005) Crystal structure of a bacterial homologue of Na^+/Cl^--dependent neurotransmitter transporters. *Nature 437*, 215–223.
38. Pao, S. S., Paulsen, I. T., and Saier, M. H., Jr (1998) Major facilitator superfamily. *Microbiol. Mol. Biol. Rev. 62*, 1–34.
39. Lindahl, E., and Sansom, M. S. (2008) Membrane proteins: molecular dynamics simulations. *Curr. Opin. Struct. Biol. 18*, 425–431.
40. Loo, T. W., Bartlett, M. C., and Clarke, D. M. (2006) Insertion of an arginine residue into the transmembrane segments corrects protein misfolding. *J. Biol. Chem. 281*, 29436–29440.
41. Guan, L., Mirza, O, Verner, G., Iwata, S., and Kaback, H. R. (2007) Structural determination of wild-type lactose permease. *Proc. Natl. Acad. Sci. U.S.A. 104*, 15294–15298.
42. Zhou, Y., Guan, L., Freites, J. A., and Kaback, H. R. (2008) Opening and closing of the periplasmic gate in lactose permease. *Proc. Natl. Acad. Sci. U.S.A. 105*, 3774–3778.